Liver-Directed Human Amniotic Epithelial Cell Transplantation Improves Systemic Disease Phenotype in Hurler Syndrome Mouse Model

NATALIE S. RODRIGUEZ,[a] LISA YANUARIA,[a] KEVIN MURPHY R. PARDUCHO,[a] IRVING M. GARCIA,[a] BINO A. VARGHESE,[b] BRENDAN H. GRUBBS,[c] TOSHIO MIKI [ID][a]

Key Words. Mucopolysaccharidosis I • Cell transplantation • Congenital • Metabolism • Amnion • Placenta

[a]Department of Surgery, Biochemistry & Molecular Biology, [b]Molecular Imaging Center, Department of Radiology, [c]Department of Obstetrics and Gynecology, Keck School of Medicine, University of Southern California, Los Angeles, California, USA

Correspondence: Toshio Miki, M.D., Ph.D., 2011 Zonal Avenue, HMR 509A, Los Angeles, California 90033, USA. Telephone: (323) 442 7703; Fax: (323) 442 4040; e-mail: toshiomi@usc.edu

ABSTRACT

Mucopolysaccharidosis type 1 (MPS1) is an inherited lysosomal storage disorder caused by a deficiency in the glycosaminoglycan (GAG)-degrading enzyme α-L-iduronidase (IDUA). In affected patients, the systemic accumulation of GAGs results in skeletal dysplasia, neurological degeneration, multiple organ dysfunction, and early death. Current therapies, including enzyme replacement and bone marrow transplant, improve life expectancy but the benefits to skeletal and neurological phenotypes are limited. In this study, we tested the therapeutic efficacy of liver-directed transplantation of a placental stem cell, which possesses multilineage differentiation potential, low immunogenicity, and high lysosomal enzyme activity. Unfractionated human amniotic epithelial cells (hAECs) were transplanted directly into the liver of immunodeficient Idua knockout mouse neonates. The hAECs engraftment was immunohistochemically confirmed with anti-human mitochondria staining. Enzyme activity assays indicated that hAECs transplantation restored IDUA function in the liver and significantly decreased urinary GAG excretion. Histochemical and micro-computed tomography analyses revealed reduced GAG deposition in the phalanges joints and composition/morphology improvement of cranial and facial bones. Neurological assessment in the hAEC treated mice showed significant improvement of sensorimotor coordination in the hAEC treated mice compared to untreated mice. Results confirm that partial liver cell replacement with placental stem cells can provide long-term (>20 weeks) and systemic restoration of enzyme function, and lead to significant phenotypic improvement in the MPS1 mouse model. This preclinical data indicate that liver-directed placental stem cell transplantation may improve skeletal and neurological phenotypes of MPS1 patients. STEM CELLS TRANSLATIONAL MEDICINE 2017;6:1583–1594

SIGNIFICANCE STATEMENT

Hurler syndrome, also known as mucopolysaccharidosis type I (MPS-I), is a rare inborn error of metabolism that results in the accumulation of glycoprotein due to a deficiency of lysosomal function. Available therapies are limited in their ability to address skeletal and neurological disease phenotypes, which are crucial for the patients' quality of life. This study in a mouse model of the disease shows that transplanted human amniotic epithelial cells (hAECs) can compensate for the missing enzyme activity long term and improve disease phenotypes, including facial bone morphology, joint mobility, and sensorimotor coordination. As hAECs are readily available nontumorigenic cells, the presenting cell therapy approach is a novel alternative for treating MPS-I Hurlers syndrome.

INTRODUCTION

Mucopolysaccharidosis type 1 (MPS1) or Hurlers syndrome is one of the most common lysosomal storage disorders and is caused by a mutation in α-L-iduronidase (IDUA; EC 3.2.1.76), a glycosaminoglycan (GAG)-degrading lysosomal exoglycosidase [1, 2]. The incidence of MPS1 has been estimated as 1 case per 100,000 live births [3]. The GAG storage disorder is systemic and heterogeneous, with various clinical manifestations including urinary excretion of excess GAG, skeletal dysplasia (broader, thicker bones, coarse facies), stiff joints, arthrogryposis and "clawed-hand" deformities, visual and auditory defects, cardiac insufficiency, organomegaly and dysfunction, progressive neurocognitive decline, and early death. The clinical spectrum ranges from the severe Hurler syndrome (MPS1-H) which is fatal within the first decade of life due to multisystem failure to the more attenuated Scheie syndrome (MPS1-

S) where patients may live into their late teens and early adulthood [4]. Mental retardation and rapid neurological and sensorimotor deterioration are hallmarks of MPS1-H, making this the variant with the most urgent need for new therapies.

Current treatments available for MPS1 patients include recombinant enzyme replacement therapy (ERT). However, the recombinant protein does not efficiently cross the blood-brain barrier, and neutralizing antibodies attenuate the efficacy of this treatment [5]. Gene therapy and hematopoietic stem cell (HSC)-based therapy have been proposed as potential new therapies. At the preclinical stage, intravenous delivery of viral vectors and gene therapy approaches have shown promise, but the residual disease still affects nervous, skeletal, and heart tissue of these same mice in adulthood [6, 7]. While HSC therapies have shown therapeutic effects on visceral organs of MPS1 mice, they do not adequately correct [8], or show only partial benefit to the neurological disease [9]. Clinical HSC transplantation also alleviated many of the disease manifestations of MPS1-H patients with the exception of neurological symptoms and bone morphology [4, 10–13]. Additionally, the morbidity and mortality associated with HSC transplantation are notable, chiefly due to rejection and graft versus host disease.

A recent combination approach utilizing HSC transplantation and gene therapy in MPS1 mice has achieved some success in this area via transplantation of IDUA overexpressing mouse and human hematopoietic progenitor cells [14, 15]. The long-term safety and efficacy of using genetically modified cells, however, remains to be determined.

Human amnion epithelial cells (hAECs) have been studied in other preclinical models of inherited metabolic diseases such as intermediate maple syrup urine disease (iMSUD) and Niemann-Pick Disease [16–18]. Importantly, upon transplantation into the livers of mice, undifferentiated hAECs have been shown to engraft, display hepatocyte-like morphology, and express various genes and enzymes normally present in mature liver, suggesting functional hepatic differentiation upon engraftment [19–21], without tumorigenicity. The human amniotic membrane has been transplanted, without immunosuppression, into the subcutaneous space of healthy volunteers and patients with lysosomal storage diseases without reported adverse effects, evidence of rejection, or tumorigenicity [22–29].

Here, we conducted a preclinical study to evaluate the therapeutic efficacy of hAEC cell transplantation in rescuing IDUA enzyme function and decreasing disease phenotype in a MPS1-H NOD/SCID murine model. Our strategy, to use hAECs to treat MPSI H via cell therapy, is innovative in that it targets the largest internal organ, the liver, as the site of cell transplantation and engraftment. Previous studies have reported that as little as 0.13% of normal IDUA activity appears to be sufficient to prevent a severe phenotype [30]. Expression of functional IDUA in even a minority of cells, via two rounds (day 2, 5) of liver-directed unfractionated hAEC injections in neonatal mouse pups, is thus a suitable goal for early intervention and correction of the classic MPS1-H biochemical phenotypes [31], measurable by tissue IDUA activity, excreted urinary GAGs, GAG accumulation in tissues, bone craniofacial morphology, and neurogenic sensorimotor coordination.

MATERIALS AND METHODS

Amniotic Epithelial Cell Isolation from Term Placenta

Human placentae were obtained from Los Angeles County +University of Southern California Medical Center with the approval of the Institutional Review Board (IRB: HS-11-00206). Only those from healthy mothers undergoing uncomplicated elective caesarean deliveries were used. All patients admitted to labor and delivery are routinely tested for Human Immunodeficiency Virus (HIV), Hepatitis B Virus (HBV), Hepatitis C Virus (HCV), Tuberculosis (TB), Chlamydia trachomatis (CT), Neisseria gonorrhoeae (GC), and syphilis. Any patient testing positive for these infectious diseases was excluded, as was any placenta showing macroscopic abnormalities or requiring detailed pathologic examination. hAECs were enzymatically isolated from the amniotic membrane as previously described, and cryopreserved [32]. An average of $200 \pm 82 \times 10^6$ cells was isolated from one placenta. Five million of these hAECs were cultured for 5–7 days to evaluate the viability, cell morphology, and proliferation rate. The remaining cells were immediately cryopreserved. In most cases, we observed that more than 95% of the cells had the cobblestone shape characteristic of amniotic epithelial cells [33]. Cells with less than 80% cell viability and more than 5% of fibroblast-like morphology of the cells were not included in this study. Cryopreserved cells were thawed and cultured for 48–72 hours before the assays for the IDUA gene, protein expression, and enzyme function were performed. These cells were also used for the cell transplantation. Three different donor-derived primary human hepatocytes were purchased from Gibco/Thermo Fisher Scientific (Gibco, Waltham, MA, www.thermofisher.com) and applied to in vitro assays as the control.

Animals

All studies were approved by the University of Southern California Institutional Animal Care and Use Committee and conducted following the NIH Guide for the Care and Use of Laboratory Animals. Breeder pairs of NOD.129(B6)-$Prkdc^{scid}$ $Idua^{tm1Clk}$ mice heterozygous for the IDUA mutation (#004083) were obtained from The Jackson Laboratory (The Jackson Laboratory, Bar Harbor, ME, www.jax.org/), housed under specific-pathogen-free conditions and provided with standard chow (TEKLAD #2018, Envigo, Huntingdon, Cambridgeshire, UK, www.envigo.com) and sterile/acidified water. Homozygous knockout (MPS1) mice start to develop disease phenotype including flattened facial profile, broadened head, thickened digits at 3 weeks of age. Severe phenotypes such as defective bone formation and broadening of the zygomatic bone have established by 8 weeks [34] (Supporting Information Fig. S2A). PCR-based genotyping was performed with specific primers according to the Jackson Laboratory's instructions.

Quantitative Single Cell Gene Expression Analysis

Single-cell gene expression analysis was performed using the Fluidigm BIOMARK HD system as per the manufacturer's recommendations (Fluidigm, San Francisco, CA, www.fluidigm.com). Briefly, single hAEC from three different placentae was sorted in each well of 96-well plates to directly synthesize cDNA from each cell (CellsDirect One-Step qRT-PCR kit, Invitrogen/Thermo Fisher Scientific). Three different donor-derived primary human hepatocytes were subjected to the same protocol to serve as controls. Fluidigm 96.96 Dynamic Array integrated fluidic circuits were used to analyze each sample for IDUA mRNA expression and compared with that of human primary hepatocytes.

Western Blotting

Mouse tissue was homogenized in 100 μl Complete Lysis M-buffer (Roche Applied Science, Indianapolis, IN, lifescience.roche.com) over ice and centrifuged for 15 minutes at 4°C 10 rpm. 20 μg total

protein samples were prepared and solubilized in Laemmli sample buffer (Bio-Rad, Hercules, CA, www.bio-rad.com) and 2-β-mercaptoethanol, separated on 4%–12% NuPAGEBis-Tris Gel 1.0, and then electrotransferred to polyvinylidene difluoride membrane using iBlot gel transfer stacks (Novex Life Technologies/Thermo Fisher Scientific). The blots were blocked with 5% Skim milk for 1 hour at room temperature. Then the blots were reacted with 1:2,000 diluted IDUA/MPS1 rabbit anti-mouse polyclonal antibody (LifeSpanBioSciences, Seattle, WA, www.lsbio.com) overnight at 4°C, washed in low salt TBST (25 mMTrisHCl pH 8.0, 150 mMNaCl, 0.1% Tween-20 [vol/vol]) three times, and reacted with horseradish peroxidase-conjugated anti-rabbit secondary antibody for 1 hour at room temperature. Finally, the blots were washed in low salt TBST and developed with WesternSure Premium Chemiluminescent substrate (LI-COR, Biotechnology, Lincoln, NE, www.licor.com) on C-DiGit Blot scanner (LI-COR).

hAEC Injections/hAEC Transplant Treatment Protocol

On day 2 and day 5 after the birth, hAECs or phosphate-buffered saline (PBS) were directly injected into the livers of neonatal mice. Prior to injection, cell viability was determined by Trypan Blue exclusion to be >90%, and enriched cell suspensions (10×10^6 cells per milliliter) were prepared with PBS. Neonate recipient mice were first anesthetized by utilizing the hypothermia induction method and placed on a paper-lined plastic dish without restraint. The maximum tolerated dose for single injection was previously determined with preliminary studies. Injection of more than a half million cells increased the mortality rate after transplantation. Therefore, a 50 μl infusion of 0.5×10^6 hAECs in PBS was administered by direct percutaneous injection into the liver pulp of neonatal mice using a sterile 30-gauge needle. A total of one million hAEC cell transplantations were performed twice on day 2 and day 5 after birth. Each cell transplantation consisted of a single injection that primarily targeted the left and median liver lobes. After transplantation, we placed the mice on a warm pad until they completely recovered. Recipient mice were then returned to their dam. Genotyping was performed post-weaning. All animals were observed and euthanized at 28 weeks.

Immunohistochemistry

Mouse livers were fixed in 4% paraformaldehyde, paraffin embedded, and sliced into 5 μm sections. Endogenous peroxidases were quenched using 0.3% hydrogen peroxide solution followed by blocking using 2.5% goat serum. Mouse anti-human mitochondrial IgG (1:1,000; Merck Millipore, Billerica, MA, www.emdmillipore.com) and horseradish Peroxidase-Conjugated goat anti-mouse IgG (1:2,000; Vector Laboratories, Burlingame, CA, vectorlabs.com) were used as primary and secondary antibodies, respectively. Bound antibodies were visualized using a peroxidase detection kit (ImmPACTNovaRED Peroxidase Substrate; Vector).

Quantitative Imaging Using Micro-CT

At 24 weeks of age, all 26 mice were imaged by the whole body computed tomography using Inveon micro-CT (Siemens Medical Solutions, Knoxville, TN, www.healthcare.siemens.com). Scans were acquired across 360°, and the X-ray settings were standardized to 80 kV and 500 μA, with an exposure time of 0.7 seconds per frame to yield a nominal resolution of 35 μm. A 0.5-mm-thick aluminum filter was used to minimize beam-hardening artifacts. Scan time for each sample was approximately 15 minutes. Subsequently, Amira 6.0 (FEI Software, Hillsboro, OR, www.amira.com)

was used to analyze bone volume and density from collected CT images. Right and left zygomatic cheekbones were targeted for comparison of bone volume and density and also normalized as a ratio of individual skull size. Results were presented using a common colormap spanning the same density range for the Untreated, WT and Treated MPS1 mice that rendered all bone densities between low bone density values (−1,000 raw CT units as red) to high bone density values (8,000 raw CT units as yellow) volume renderings of bone density. Mineral density was calibrated in units of mg HA/cc using a standard hydroxyapatite phantom (Scanco Medical AG, Bruettisellen, CH, Switzerland, www.scanco.ch). Volume was measured as the product of the number of voxels comprising the zygomatic bone and the voxel resolution.

Urinary GAG Excretion

Urine samples were collected weekly by using diuresis cages (Tecniplast, West Chester, PA, www.tecniplast.it/us), diluted, and frozen at −20°C until analyzed. GAG concentration in the urine was determined by the 1,9-dimethylmethylene blue (DMMB; Sigma–Aldrich, St. Louis, MO, www.sigmaaldrich.com) method. Serial dilutions of urine (25 μl) were mixed with 25 μl of 0.48 M guanidine HCl and 200 μl of the DMMB dye and measured as previously described in two protocols [31, 35]. The absorbance value was determined as ΔA= Abs$_1$ 550 nm–Abs$_2$ 650 nm. GAG concentration was calculated using a standard curve generated from heparan sulfate standards. Urinary creatinine concentration was selected as the normalizing value [36, 37] and determined using a colorimetric picric acid endpoint enzymatic assay kit (Crystal Chem, Downers Grove, IL, www.crystalchem.com). Urinary GAG excretion was expressed as μg GAG/mg creatinine for each urine sample.

Alpha-ʟ-Iduronidase Activity Assay

Sodium formate, formic acid, 4-methylumbelliferone, glycine, NaOH, Triton X-100 and sodium azide were obtained from Sigma and 4-methylumbelliferyl alpha-ʟ-iduronide from Glycosynth (Warrington, Cheshire, U.K., www.glycosynth.co.uk).

For Organ IDUA Activity: After sacrifice using isoflurane, mice were perfused transcardially with cold PBS. Samples from the brain (and cerebellum), heart, kidney, liver (all lobes), spleen, and lungs were immediately harvested and flash-frozen for IDUA and GAG analysis. Harvested mouse tissues were placed in 1 ml PBS in a microcentrifuge tube on ice and homogenized using a motorized pestle.

For Intracellular IDUA activity in Cultured Cells/Frozen Hepatocytes: Cells were homogenized by ultrasonic sonication (QSonica Q700, Newtown, CT, www.sonicator.com) in 100 μl cold PBS over ice at a pulse mode rate of 10 seconds, three times, at 40% amplitude and set temperature of 4°C. Homogenate was centrifuged for 10 minutes at 4°C, 13,000 rpm to recover cytosolic protein IDUA enzyme. 10% Triton X-100 in PBS was added, and the homogenate (tissue/cell) kept on ice for 10 minutes. Protein concentration in the clarified supernatant was estimated by the Bradford colorimetric method. Briefly, 25 μl of a solution of 50 μM 4-methylumbelliferyl alpha-ʟ-iduronide made in 0.4 M sodium formate buffer, pH 3.5, containing 0.2% Triton X-100 was added to 25 μl of tissue homogenate and incubated for 1 hour at 37°C in the dark. The reaction was quenched by adding 200 μl of 0.5 M NaOH/glycine buffer, pH 10.3. Tubes were centrifuged for 1 minute at 13,000 rpm at 4°C, the supernatant transferred to a 96 wells plate, and fluorescence read at 365 nm excitation wavelength and 450 nm emission wavelength using a SpectraMax M5 fluorometric plate reader (Molecular Devices, Sunnyvale, CA,

www.moleculardevices.com). IDUA activity in the tissue samples was calculated as: activity in ng/hour = (fluorometric reading of the tissue sample × A)−B, where A and B were the values obtained from the curve fit the equation of standard curve generated using pure end product (4-methylumbelliferone). The specific activity of IDUA was expressed as nmol/hour/mg protein in each sample.

Alcian Blue/Alizarin Red Adult Mouse Skeletal Staining and Limb Measurements

After euthanizing mice at 28 weeks, forelimbs and hind limbs were collected and fixed in 70% ethanol for 1–2 weeks. Skin and hair were removed, and limbs were fixed in 95% ethanol for several days. Limbs were stained with Alcian Blue solution: 20 mg Alcian Blue 8 Gx, 70 ml 100% ethanol, 30 mL glacial acetic acid, all from Sigma-Aldrich, shielded from light, for 12 days. When satisfied with the darkness of blue, specimens were digested with 2% potassium hydroxide for 4 days, cleaned, soaked in 95% ethanol overnight, and stained with Alizarin Red solution (100 ml 1% potassium hydroxide, 6 mg Alizarin Red, all from Sigma-Aldrich) for overnight. Staining was stopped with 70% ethanol overnight. Specimens were stored in 50% Glycerol: 50% ethanol solution. Forelimb third metacarpal and proximal phalanges, as well as hindlimb third metatarsal and proximal phalanges for wild-type, untreated, and treated mice were visualized and photographed using Olympus SZX16 Stereo Microscope (Olympus, Waltham, MA, www.olympus-lifescience.com) and SPOT Advanced Plus Software 5.0 (SPOT Imaging, Sterling Heights, MI, www.spotimaging.com/). Quantification of bone length, width, and volume was done using ImageJ Software.

Rotarod Test for Sensorimotor and Behavioral Testing

A rotarod apparatus (ROTOR-ROD Model for Mice, San Diego Instruments, San Diego, CA, www.sandiegoinstruments.com) was used to measure the ability of WT, MPS1 homozygous untreated, and treated mice to remain balanced on a rotating rod (3.2 cm diameter) at four different speeds. Mice used in this experiment were 23 weeks of age and naïve to the test. A total of 13 mice (4 WT, 4 untreated, and 5 treated were tested. Mice were first individually habituated to the stationary rod for 180 seconds, then tested at incremental speeds of 5, 15, 25, or 35 rpm three trials at each speed for 5 consecutive days. Mean scores of the three trials at each speed were calculated. Latency to fall (in seconds) was scored for each animal at each speed in each trial. Seven photo beams per lane below the running rod assured that only true falls were recorded on ROTOR-ROD software per trial. Animals rested 10 minutes between trials to prevent fatigue and exhaustion. The test requires a high degree of sensorimotor coordination and acquisition of motor skills. The initial test served as a measure of baseline sensorimotor function, and impairment is indicative of damage to the basal ganglia and cerebellum [31]. Patterns of improvement or decrement in motor coordination were assessed by repeating the testing on five consecutive days.

Statistical Analysis of IDUA Activity, Urine GAG levels, and Cheekbone Micro-CT Analysis

Results are expressed as mean ± standard error of the mean (SEM). All assays were repeated at least three times with two biological replicates and three technical replicates. Statistical analysis was performed with Prism 6.0h (GraphPad Software, San Diego, CA, www.graphpad.com). Experimental and control groups were compared with unpaired Student's t test or one-way analysis of variance (ANOVA) (with Bonferroni post hoc analysis and Tukey's multiple comparison). A value of $p < .05$ was considered statistically significant.

RESULTS

Primary Human Amniotic Epithelial Cells Possess IDUA Enzyme Function

The IDUA gene and protein expression and the enzyme activity in unfractionated hAECs were compared with that of primary human hepatocytes by single-cell quantitative RT-PCR, Western blot analysis, and IDUA activity assay, respectively (Fig. 1). Prior to these analyses, the protein homology of human IDUA and mouse Idua was confirmed (Supporting Information Fig. S1). Single cell qRT-PCR analyses were conducted with samples from three individuals. The data revealed that *IDUA* gene expression of hAECs is overall equivalent to that of human primary hepatocytes (Fig. 1A). In fact, hAECs contain more IDUA protein per total cellular protein than do hepatocytes as assessed by Western blot (Fig. 1B). In vitro activity of IDUA enzyme isolated from hAECs was equivalent to slightly higher than that of IDUA isolated from primary hepatocytes, as normalized to total IDUA protein in the assay (Fig. 1C). Cultured hAECs were also probed for lysosomal IDUA and lysosome-associated protein-1 (LAMP1), which confirmed the presence of abundant IDUA containing lysosomes in hAECs (Supporting Information Fig. S1B). Liver-directed cell transplantation was performed by direct percutaneous injection of 0.5×10^6 unfractionated hAECs into the liver parenchyma. A total of 1 million hAECs were administered in two doses, at days 2 and 5 after birth (Fig. 1D). hAEC transplanted MPS1 homozygous mice (Treated), PBS injected MPS1 homozygous (Untreated), and wild-type littermates (WT) were observed for 24 to 28 weeks with weekly urine collection beginning at 8 weeks to assess GAG excretion levels. Sensorimotor rotarod 5-day training was performed at 24 weeks, followed by micro-computed tomography (micro-CT) imaging for bone morphology analysis, and sacrifice for tissue enzymatic assay and histology. Engraftment of human cells in mouse liver was confirmed by immunohistochemically staining human mitochondria in the recipient mouse liver (Fig. 1E, 1F, Supporting Information Fig. S2B–S2F).

Restoration of IDUA Enzyme Function in MPS1 Homozygous Mice After hAEC Transplantation

From 8 to 24 weeks, urine GAG concentrations of WT, Untreated, and Treated mice were analyzed. MPS1 Treated mice demonstrated a significant decrease (3.1-fold) of urine GAG levels compared to MPS1 Untreated mice, $p < .0001$ (Fig. 2A). MPS1 Treated mice demonstrated consistently lower urinary GAG levels than untreated mice during the observation period (Fig. 2B). The time course data indicated that stable functional recovery of IDUA enzyme was mediated by the hAEC transplantation. At the experimental endpoint, IDUA activity was biochemically assayed in six major organs including liver, kidney, lung, spleen, heart, and brain. Although there was a trend toward higher IDUA enzyme activities in all six organs of MPS1 Treated mice, the differences were not statistically significant except in the liver (Fig. 2C). Liver IDUA enzyme activity was significantly restored in all treated mice compared to untreated mice ($p < .05$). However, the enzyme activity was still 75% lower than was seen in the livers of WT mice (Fig. 2D). Liver histology by Alcian Blue staining of acidic
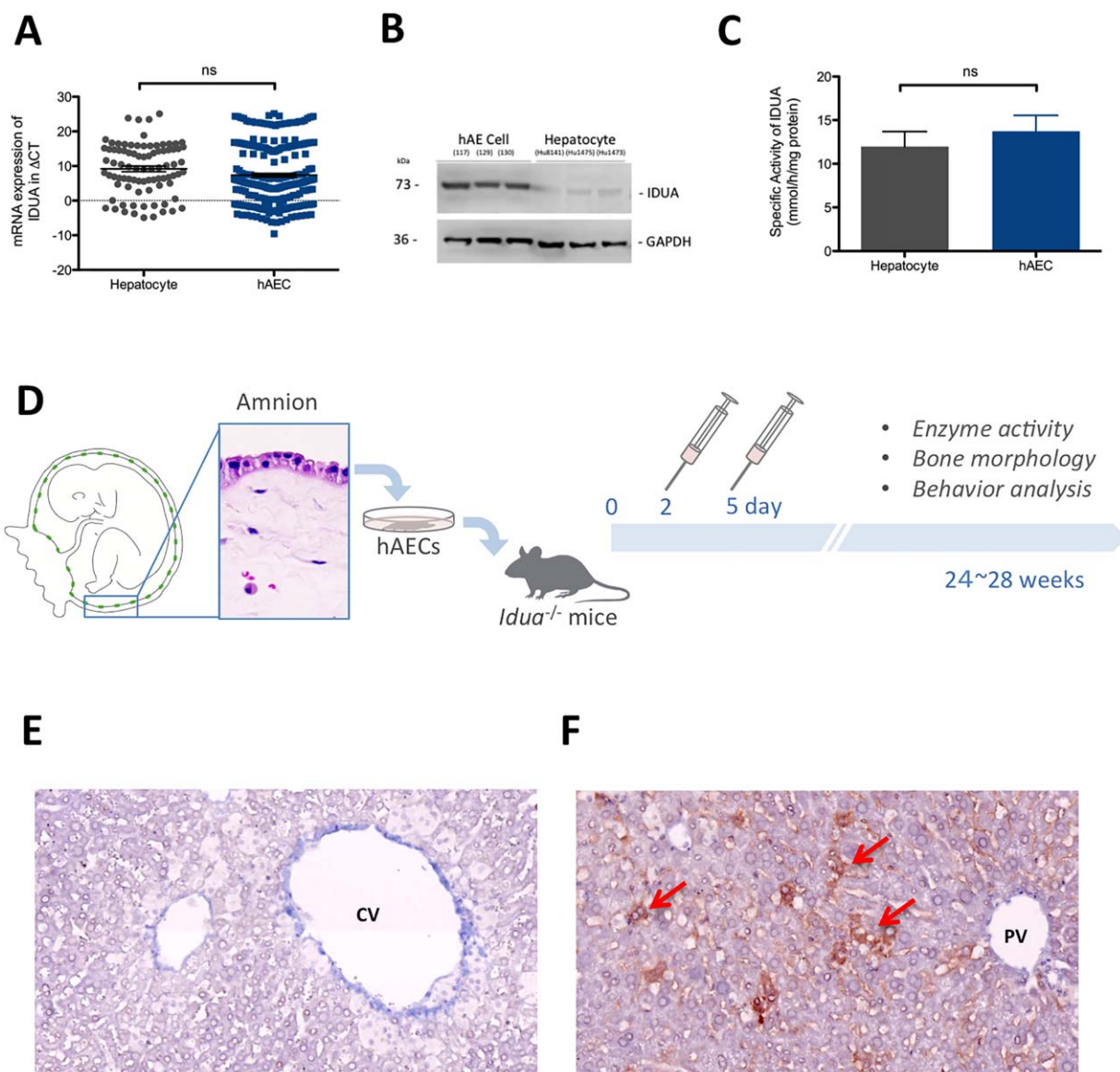
Figure 1. Primary hAEC characterization and the liver-directed cell transplantation. **(A)**: Single cell gene expression data reveal *IDUA* gene expressions in hAECs is equivalent to that of primary human hepatocytes. Delta-Ct values were calculated from the difference in the Ct of IDUA and that of three housekeeping genes: GAPDH, beta-actin, and cyclophilin A. Each dot represents the delta-Ct value of a single cell that was isolated from three different placentae. Three different primary human hepatocytes purchased from Gibco/Thermo Fisher Scientific were used as the control. **(B)**: Western blot analysis demonstrated that hAECs contain more IDUA protein than hepatocytes. **(C)**: In vitro IDUA enzyme activity is not significantly different in hAEC and primary hepatocytes. Mean $\pm$ SEM were graphed. (ns $p = .9543$, Unpaired Student's t test). **(D)**: The schematic shows an overview of the experimental procedure. The amniotic epithelial cells were enzymatically isolated from the innermost lining of placenta (H&E staining). The isolated cells were cryopreserved immediately and thawed 48–72 hours before cell transplantation. A total of one million hAECs were transplanted twice by direct percutaneous injection into the neonate mouse liver parenchyma at days 2 and 5 after birth. Mice were observed until 28 weeks after the transplantation. At 28 weeks after liver-directed injection, NOD/SCID MPS1 mice were euthanized, livers were processed for histology, and engrafted human cells were detected using a mouse anti-human mitochondrial antibody with NovaRED peroxidase substrate. The panel shows PBS injected control mouse liver **(E)** and hAEC injected mouse liver **(F)**. Abbreviations: CV, central vein; GAPDH, glyceraldehyde-3-phosphate dehydrogenase; hAECs, human amniotic epithelial cells; IDUA, α-L-iduronidase; PV, portal vein.

mucopolysaccharides/GAGs in tissue did not demonstrate notable improvement in the lobes sampled, with some persistence of staining surrounding portal and central veins (Fig. 2E). Staining of brain (striatum), cerebellum, and kidney tissue revealed a minor decrease in GAG inclusions in the treated MPS1 mice compared to those not treated (Supporting Information Fig. S3A–S3D). No tumor formation was observed in any organs in a total of 96 recipient mice throughout this study. Although we did not observe immediate death after cell transplantation, the overall mortality in the transplanted neonatal animals was 6.25%.

## Bone Morphology and Quality Analysis by High-Resolution Micro-CT

Craniofacial and skeletal disorders, such as thickened calvaria and poor long bone remodeling with shortened, irregular wide shafts, are hallmarks of the MPS1 clinically and in the mouse model. In
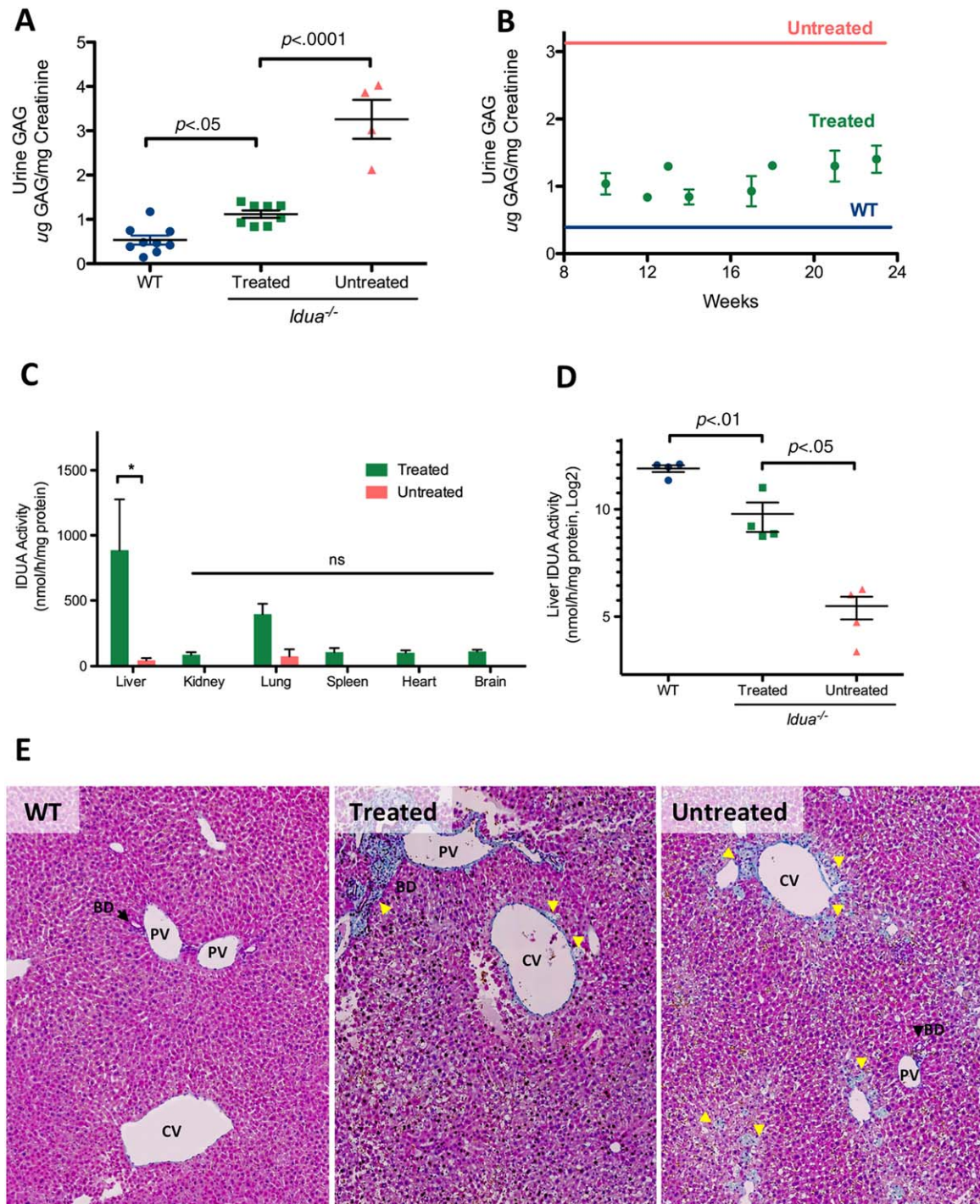
Figure 2. Restoration of IDUA enzyme function in MPS1 homozygous mice after human amniotic epithelial cells (hAECs) transplantation. **(A)**: hAEC transplanted MPS1 homozygous (Treated) mice demonstrated significant decrease of urinary GAG concentration. **(B)**: Throughout the monitoring period of 8 to 24 weeks, urinary GAG concentrations of treated mice were consistently lower than untreated mice. The average urinary GAG concentrations of untreated mice (3.112 ± 1.850 µg GAG/mg creatinine) and wild type (0.531 ± 0.357 µg GAG/mg creatinine) were supplementally presented in red and blue straight lines, respectively. **(C)**: Tissue IDUA activity was biochemically assayed in six major organs including liver, kidney, lung, spleen, heart, and brain. While IDUA enzyme activities were higher in all organs of treated mice, the differences were not statistically significant except in the liver. Mean $\pm$ SEM were graphed (*, $p < .05$, Unpaired Student's t test). **(D)**: Although liver IDUA enzyme activity was significantly restored by hAEC transplantation, it was still significantly lower than the wild type mouse liver. Mean $\pm$ SEM were graphed. $n = 26$. **(E)**: Liver histology (Alcian Blue staining of mucopolysaccharides and nuclear fast red counterstain) did not demonstrate notable decreases in GAG accumulation (indicated by yellow arrows). Abbreviations: BD, bile duct; CV, central vein; GAG, glycosaminoglycan; IDUA, α-L-iduronidase; PV, portal vein; WT, wild type.
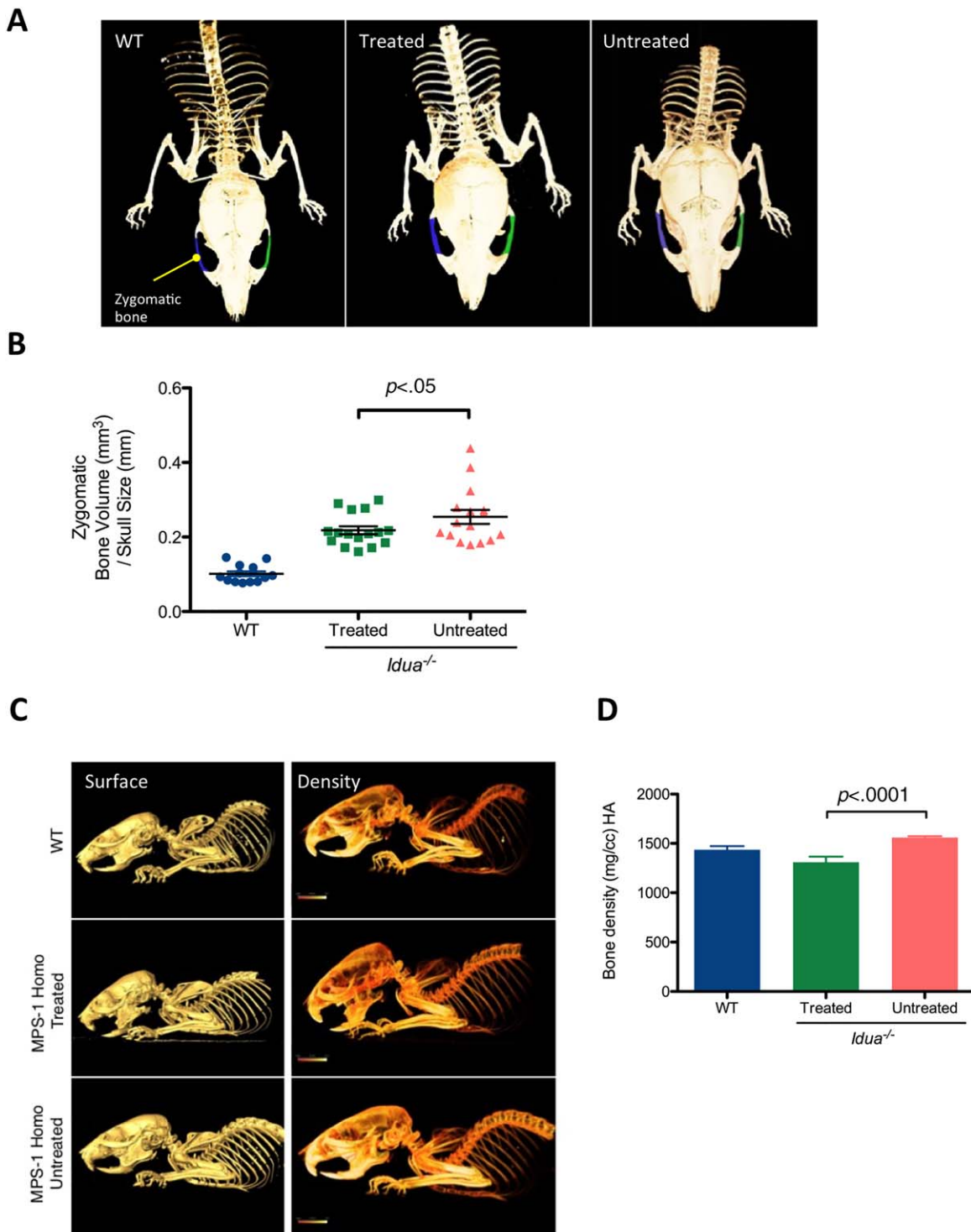
Figure 3. Bone morphology and quality analysis by high-resolution X-ray micro-computed tomography (micro-CT). **(A):** Increased zygomatic bone volume is a signature phenotype of homozygous *Idua* knockout (MSP1) mice. We measured both right (blue) and left (green) zygomatic bone volume and density using micro-CT derived virtual models. **(B):** Zygomatic bone volume was significantly decreased in treated mice. Volume measured as the product of the number of voxels making the zygomatic bone and the voxel resolution. Each dot represents zygomatic bone volume normalized with skull size. $n = 26$. **(C):** Sagittal view bone surface renderings reveal the short, flattened nose phenotype in untreated and to a lesser extent, treated mice. Comparative analysis of the volumetric bone density distribution reveal higher bone density level in the untreated mouse skull compared to WT and treated mouse. The results were presented using a common colormap across the untreated WT and treated mice that rendered all bone densities between low bone density value ($-1{,}000$ raw CT units as red) to high bone density values ($8{,}000$ raw CT units as yellow) volume renderings of bone density. Note the increase in the amount of yellow in the untreated compared to WT and treated mouse. **(D):** HA density per a cubic centimeter indicated statistically significant differences between treated and untreated groups. Mineral density was calibrated in units of mg HA/cc using a standard hydroxyapatite phantom (Scanco Medical AG). Mean $\pm$ SEM were graphed, $n = 26$. Abbreviations: HA, hydroxyapatite; MPS1, mucopolysaccharidosis type 1; WT, wild type.
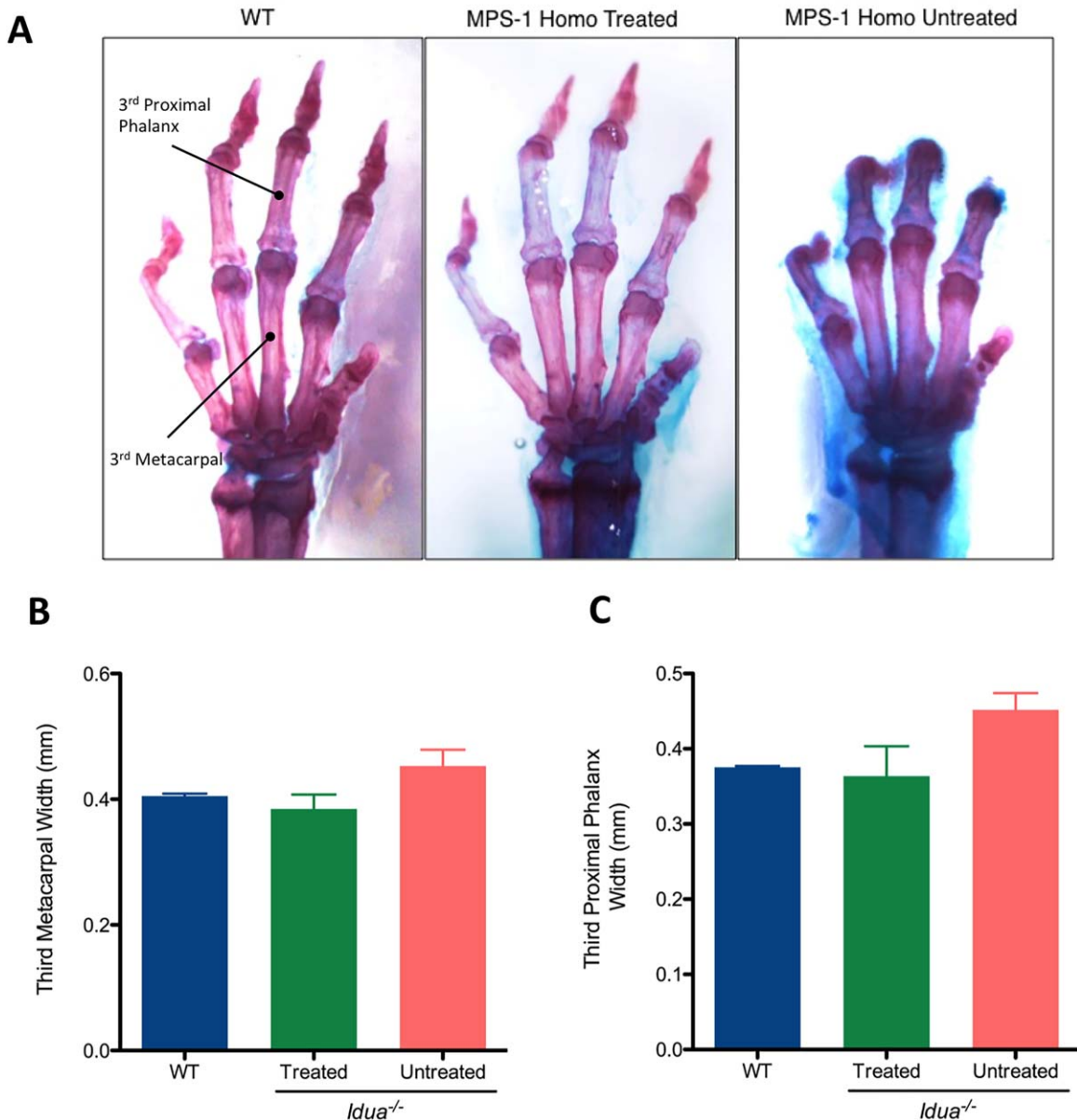
Figure 4. Limb skeletal morphology in MPS1 mice demonstrated by Alizarin Red and Alcian Blue staining. **(A)**: Forelimbs of WT; MPS1 homozygous treated (Treated); and MPS1 Homozygous (Untreated) mice were stained with Alizarin Red (bone) and Alcian Blue (acid mucopolysaccharides). Arthrigryposis in the first and second joints of the forelimb with "claw-shaped" hand as well as thicker connective tissue deposition were seen in the MPS-1 homozygous untreated mice. The width of the third metacarpal **(B)** and proximal phalanges **(C)** were not statistically significant different between groups, though slight improvement was seen in treated mice versus untreated mice (Mean $\pm$ SEM, $n = 14$ per group, $p = .1021$). Abbreviations: MPS1, mucopolysaccharidosis type 1; WT, wild type.

humans, the constellation of skeletal dysplasia and spinal abnormalities (the latter not seen in the mouse model) are known as the dysostosis multiplex. In the mouse model, widening of the zygomatic arches, foreshortening of the premaxillary bones, and enlargement of the cranium have been especially well-documented [31, 34, 38, 39]. The increasing zygomatic bone volume and density in fact, is a signature phenotype of Idua$^{-/-}$ MPS1 mice [31] and was thus selected as a point of comparison for our study. We performed 3D morphometry measurements for both right (blue) and left (green) zygomatic bone volume and density using micro-CT (Fig. 3A). Zygomatic bone volume was significantly decreased in treated mice (Fig. 3B). Dot plots of individual

zygomatic bone volumes indicate that hAEC transplantation improved the extremely high volume group disease mice more so than the mild phenotype mice. Sagittal views of 3D bone surface rendering reveal the shortened nose phenotype in treated and untreated MPS1 mice. Bone density images reveal slightly higher bone density levels in the untreated mouse skull (Fig. 3C, Supporting Information Fig. S4A). Statistical analysis (one-way ANOVA, $p < .0001$) of the quantified hydroxylapatite density of the skull (HA: mg/cc) demonstrated a significantly lower bone density in the hAEC treated group (1,309.90 $\pm$ 223.93 mg/cc) as compared to the untreated group (1,559.37 $\pm$ 51.50 mg/cc) (Tukey's multiple comparison test, $q = 6.412$) (Fig. 3D).
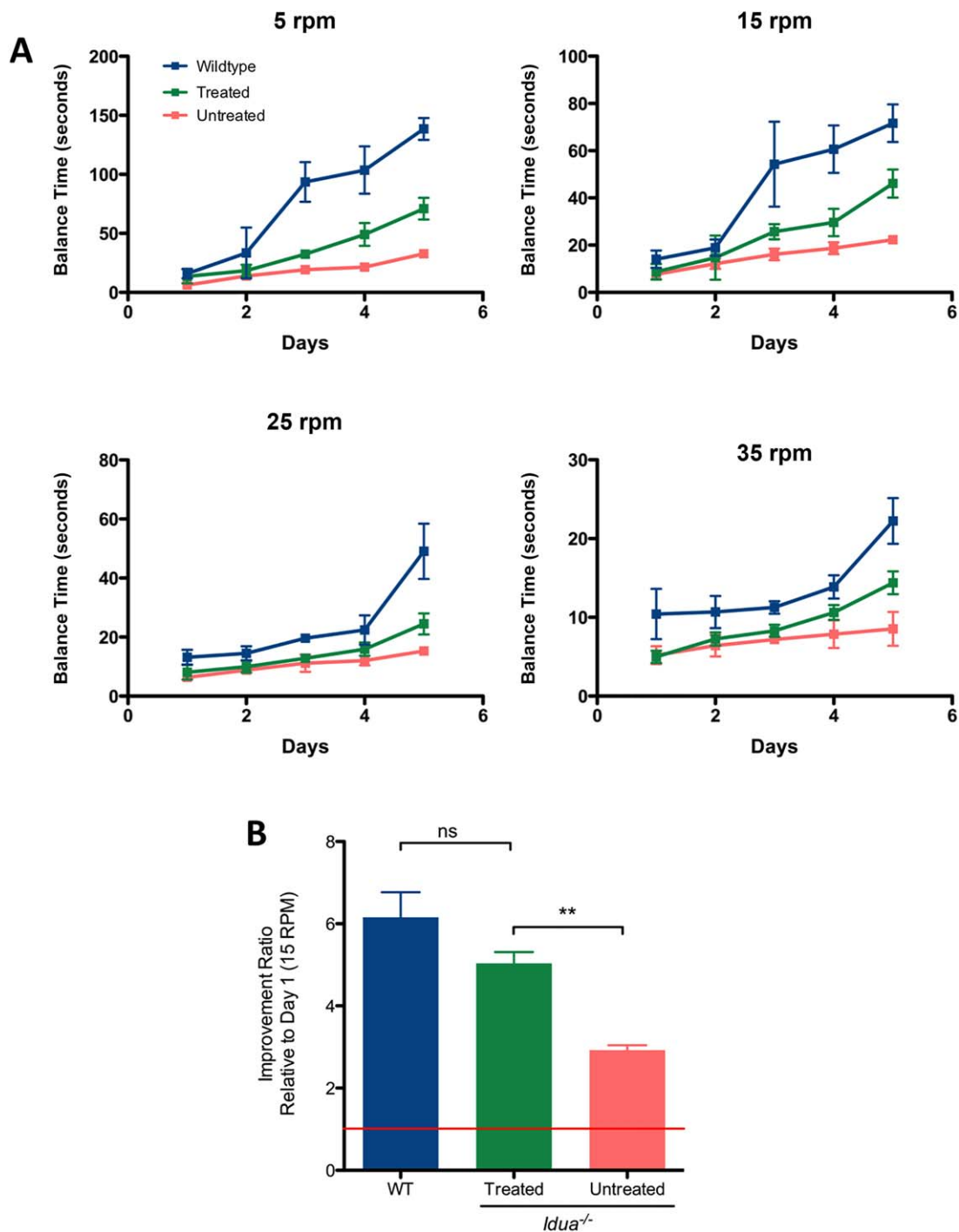
Figure 5. Rotarod performance test showing behavioral phenotype improvement in the human amniotic epithelial cells (hAECs) transplanted mice. **(A)**; Wild type (WT; Blue), mucopolysaccharidosis type 1 (MPS1) homozygous treated (Treated; Green) and MPS1 homozygous (Untreated; Red) were trained on the rotarod for 5 days at 4 different rotation speeds (5, 15, 25, 35 rpm). All mice were 23 weeks of age and naive to the rotarod test. With all tested speeds on the rotarod, the treated mice showed improvement in motor coordination skills. **(B)**: After 5 days of a learning period, the improvement ratio was significantly higher in the hAEC-transplanted mice (green) compared to untreated (red) mice at a speed of 15 rpm. The improvement was demonstrated as relative to Day 1 balance time. There was no significant difference between wild type mice and treated mice. Mean $\pm$ SEM were graphed (ns $p \geq .05$, **, $p < .01$, one-way ANOVA).

Limb Skeletal Morphology in MPS1 Mice Demonstrated by Alizarin Red and Alcian Blue Staining

In human MPS1 disease, joints often become stiffened by the age of two years, with progressive arthropathy universally affecting the joints and leading to poor hand function and range of motion. The hands commonly take on a characteristic joint contracture deformity resulting from both phalangeal dysostosis and synovial thickening. Similarly, untreated MPS1 mice show arthrogryposis in the first and second joints and a "clawed hand" phenotype, as well as thicker connective tissue

deposition, visible by Alcian Blue staining (Fig. 4A). The width of the third metacarpal (Fig. 4B) and proximal phalanges were measured and plotted. Although the average width of MPS1 Treated group (third metacarpal: 0.384 ± 0.045, proximal phalanx: 0.364 ± 0.079) was shorter than the MPS1 Untreated group (third metacarpal: 0.453 ± 0.052, proximal phalanx: 0.452 ± 0.045), there were no statistically significant differences. However, there was remarkable improvement of joint contractures. Whereas most of the connective tissue in the WT and the MPS1 Treated groups' forehands dissolved after 2% potassium hydroxide process, the MPS1 Untreated group revealed a large volume of adherent connective tissue deposition from the wrist to the distal interphalangeal joints. As a result, the interphalangeal joints of MPS1 Treated group were more easily movable than the MPS1 Untreated group, comparable to those of the WT group. While these differences were observed during quiet home cage behavior evaluation and handling, the differences in ease of mobility were not quantified.

Rotarod Performance Test Showing Behavioral Phenotype Improvement in the hAEC Transplanted Mice

Progressive mental retardation is a hallmark of MPS1 in human patients, though the exact mechanisms are not completely understood, they appear to involve neuron loss with atrophy, altered neuronal structures, and obstruction of cerebrospinal fluid reabsorption [40–42]. There is extreme heterogeneity in the severity of developmental and intellectual manifestations. Both the human disease and mouse MPS1 model demonstrate progressive accumulation of GAG material in the brain. Previous MPS1 mouse studies have shown defective sensorimotor integration involving the cerebellum, striatal, and proprioceptive pathways and the cerebral cortex, as well as impaired acquisition of motor coordination [31]. These abnormalities are correlated with the location of neuropathological changes, demonstrated by Alcian Blue staining GAG accumulation in the brain, particularly in the cerebellum (Supporting Information Fig. S3C, S3D). Sensorimotor function and motor coordination learning capabilities of hAEC treated mice were thus evaluated by rotarod performance test over 5 consecutive days of training. Whereas reproducible abnormalities in the sensorimotor function and abnormal motor coordination learning were observed in the MPS1 Untreated mice, MPS1 Treated mice demonstrated significant ($p < .01$) improvement in both motor coordination with increasing speed and learning, and improved balance times from day 1 to day 5 (Fig. 5, Supporting Information Fig. S4B). Wild-type mice were expected to remain on a rotating bar (rotarod) for longer periods of time than the MPS1 Untreated mice, with the differences increasing with higher rotational speeds. At all of the tested speeds (5, 15, 25, 35 rpm), the MPS1 Treated mice demonstrated improvement in motor coordination skills compared to MPS1 Untreated mice (Fig. 5A). At 35 rpm, MPS1 Untreated mice appeared unable to improve much over the course of 5 days. On day 1 of training at each of the four speeds, MPS1 Untreated mice were able to balance on the rotarod for less than half as long as WT, and less than MPS1 Treated mice. By day 5 of training, WT and MPS1 Treated mice were able to remain balanced on the rotarod for longer at the higher speeds. The performance of MPS1 Untreated mice improved slightly but never became equal to that of WT or MPS1 Treated mice. The improvement rate of MPS1 Untreated mice over the course of the 5-day training was also lower than WT and MPS1 Treated mice. At speeds of 15 rpm in fact, the improvement ratio was significantly

higher (one-way ANOVA analysis of variance, $p = .003$) in the MPS1 Treated mice compared to MPS1 Untreated mice. There was no significant difference between WT and MPS1 Treated mice at this speed (Fig. 5B). We observed, but did not quantify, that the overall behavior of hAEC treated mice was improved. On quiet home cage evaluation nearing the endpoint of this study, these mice were actively grooming, eating, drinking, and interacting with their cage mates. This was more comparable to WT behavior than to that of their untreated/PBS injected counterparts, which displayed the MPS1 phenotype of rough fur, weaker forelimb grip on cage bars, along with slower movements.

DISCUSSION

Our study demonstrates the therapeutic efficacy of hAEC transplantation into the neonatal livers of the MPS1 disease mouse model. Throughout the 28 weeks of extended post-transplantation observation period, treated mice showed significant improvement in multiple aspects of the disease phenotype. In addition to significantly increasing the level of IDUA activity in the liver and lowering urine GAG concentration, treatment correlated with improved neurological performance and bone density. Previous studies have shown that excess GAG accumulation inhibits the degradation of collagen type II by cathepsin K, resulting in impaired osteoclast activity and decreased cartilage resorption. This contributes to the skeletal abnormalities seen in the MPS1 human disease and the mouse model [43, 44]. Significant normalization of bone volume and density values in our treated mice is further evidence of the therapeutic reduction of systemic GAGs achieved via liver-directed hAEC transplantation. The decreased severity of joint contractures indicates that the treated mice regained some level of flexibility and mobility in their forehands compared to untreated mice. Combined with the significant improvement in sensorimotor coordination and learning capabilities, these results suggest that the hAEC transplantation possesses tremendous potential to improve patients' quality of life.

hAECs possess four unique properties: low immunogenicity [29], immunomodulatory/anti-inflammatory activity [45, 46], multilineage differentiation potential [24, 33, 47], and they are lysosome-rich cells [18, 27, 48]. These properties have attracted clinicians and researchers looking for an appropriate, more abundant cell source to treat congenital metabolic liver disorders where a single enzyme function is defective or lost. The therapeutic efficacy of hAEC transplantation has been shown with other congenital metabolic disorder mouse models. Skvorak et al. transplanted hAEC directly into the liver of iMSUD neonate mice [16, 17]. Whereas untreated control mice die within 40 days after their birth, hAEC transplanted disease mice survived more than 100 days. An intraparenchymal liver delivery approach using hAECs is thus reasonable and successful for liver-specific metabolic disorders. While our targeted disease MPS1 is, unlike iMSUD, a systemic disorder, we hypothesized that expression of the enzyme in the liver, the largest internal organ and a reservoir of lysosomes and IUDA producing cells, would be sufficient to rescue many of the systemic defects and disease phenotypes. To this end, the differentiation capability of hAEC into hepatocytes was not crucial as long as the IDUA enzyme activity was equivalent or superior to the native hepatocytes. As we demonstrated, the naive hAECs express the IDUA gene and protein in sufficient quantity.

hAEC transplantation has advantages to traditional therapies such as ERT. Clinical ERT studies with MPS-1 patients have shown

the development of anti-laronidase IgG antibodies during the first months of treatment. However, evolving tolerance resulted in an IgG reduction at 2 years of treatment [49, 50]. Therefore, while we may observe an increase in initial antibody titer, we anticipate that this will likely not cause a problem in the long term. In addition, the IDUA enzyme will be enclosed inside the lysosomes of hAECs, which have shown low immunogenicity [29]. This may further limit exposure to the host immune system and subsequent antibody development, which would maximize IDUA levels.

In the clinical setting, the required number of cells for therapeutic efficacy will be dependent on the case. The patient's age, the level of enzyme function, and the degree of GAG accumulation will vary and will need to be considered to determine the appropriate dose of donor cells. Until we obtain sufficient clinical data, the most practical approach will be to start with a small quantity of cells and then repeat the cell transplantation until overall IDUA function is restored to a normal threshold value. Unlike transplantation of whole organs and hematopoietic stem cells, AEC transplantation requires a minimally invasive procedure, which can be repeated without excess burden on the patient. A gene therapy study using the same mouse model demonstrated that an expression level of 1% normal IDUA activity in the liver was sufficient to reduce the GAG level in liver, spleen, kidney, heart, and lung [51]. Studies using fibroblasts from individuals with MPS I have revealed that as little as 0.13% of normal IDUA activity appears to be sufficient to produce a mild phenotype [30]. In this study, we demonstrated that injecting hAECs to achieve approximately 1.5% of total mouse neonate liver cells showed up to 25% of IDUA enzyme recovery, which is greater than the activity of mild phenotype patients. About 200 million hAECs can be isolated from one placenta, which is considerably higher than other sources of stem cells. Our previous in vitro study indicated that these cells are able to propagate over 10 passages [33]. Although we have not tested the IDUA activity of these expanded hAECs, in theory, more than two hundred billion cells will be available from one placenta.

This study showed that the transplanted hAECs engrafted in the recipient liver and metabolized excess GAGs produced by the neighboring diseased hepatocytes. In addition to the expected enzyme activity in the liver, a slight increase of IDUA activity was observed in other organs including the brain. As the transplanted cells were not able to pass the blood-brain barrier, this observation may be explained by hAEC-derived vesicles such as exosomes. In fact, increasing evidence suggests that intracellular exosome transfer contributes to the therapeutic efficacy of cell transplantation for diseases such as myocardial ischemia and infarction [52–54] and MPS VII corneal defects [55]. Further studies are required to determine the cell-to-cell communication involved in the therapeutic mechanism of hAEC transplantation and IDUA delivery. Once this therapeutic mechanism is defined, the next step will be to reproduce this therapeutic efficacy with hAEC isolated under current Good Manufacturing Practices (cGMP) conditions. We envision that the clinical hAEC transplantation will be conducted with the protocol that has been established for clinical hepatocyte transplantation, utilizing the umbilical vein to transplant HLA-matched AECs into the newborn liver. For Hurler syndrome patients, cell transplantation should ideally be performed as soon as it is diagnosed and prior to reaching pathologic levels of GAG.

CONCLUSION

In summary, our study demonstrates the therapeutic efficacy of hAECs for MPS1 Hurlers Syndrome. This cell replacement approach targeting the liver with previously established hepatocyte transplantation protocols could provide a viable and efficacious therapy for patients who suffer congenital metabolic lysosomal storage disorders.

AUTHOR CONTRIBUTIONS

N.S.R.: design and performed the experiments, financial support, manuscript writing; L.Y.: performed mice colony breeding and cell injections, sample preparation, cell isolation from human term placentae; K.M.R.P.: performed immunohistochemical analyses; I.M.G.: performed mice colony breeding and cell injections, sample preparation, cell isolation from human term placentae; B.A.V.: performed MicroCT imaging and data collection and analysis; B.H.G.: collection of placentae and manuscript writing; T.M.: conception and design, financial support, manuscript writing, final approval of manuscript.

DISCLOSURE OF POTENTIAL CONFLICTS OF INTEREST

T.M. is a shareholder of NoveomeBiotherapeutics, Inc. The authors have received no payment for the preparation of this manuscript and state no other financial and non-financial conflict of interests.

REFERENCES

1 Dorfman A, Matalon R. The mucopolysaccharidoses (a review). Proc Natl Acad Sci USA 1976;73:630–637.

2 Bie H, Yin J, He X et al. Insights into mucopolysaccharidosis I from the structure and action of α-L-iduronidase. Nat Chem Biol 2013;9:739–745.

3 Meikle PJ, Hopwood JJ, Clague AE et al. Prevalence of lysosomal storage disorders. JAMA 1999;281:249–254.

4 Wraith JE, Jones S. Mucopolysaccharidosis type I. Pediatr Endocrinol Rev 2014; 12(suppl 1):102–106.

5 Pastores GM. Laronidase (Aldurazyme): Enzyme replacement therapy for mucopolysaccharidosis type I. Expert Opin Biol Ther 2008;8:1003–1009.

6 Herati RS, Ma X, Tittiger M et al. Improved retroviral vector design results in sustained expression after adult gene therapy in mucopolysaccharidosis I mice. J Gene Med2008;10:972–982.

7 Ma X, Liu Y, Tittiger M et al. Improvements in mucopolysaccharidosis I mice after adult retroviral vector–mediated gene therapy with immunomodulation. Mol Ther 2007;15:889–902.

8 Zheng Y, Rozengurt N, Ryazantsev S et al. Treatment of the mouse model of mucopolysaccharidosis I with retrovirally transduced bone marrow. Mol Genet Metab 2003;79:233–244.

9 Wang D, Zhang W, Kalfa TA et al. Reprogramming erythroid cells for lysosomal enzyme

production leads to visceral and CNS cross-correction in mice with Hurler syndrome. Proc Natl Acad Sci USA 2009;106:19958–19963.

10   Staba SL, Escolar ML, Poe M et al. Cord-blood transplants from unrelated donors in patients with Hurler's syndrome. N Engl J Med 2004;350:1960–1969.

11   Ru MH de, Boelens JJ, Das AM et al. Enzyme replacement therapy and/or hematopoietic stem cell transplantation at diagnosis in patients with mucopolysaccharidosis type I: Results of a European consensus procedure. Orphanet J Rare Dis 2011;6:55.

12   Miebach E, Church H, Cooper A et al. The craniocervical junction following successful haematopoietic stem cell transplantation for mucopolysaccharidosis type I H (Hurler syndrome). J Inherit Metab Dis 2011;34:755–761.

13   Schmidt M, Breyer S, Löbel U et al. Musculoskeletal manifestations in mucopolysaccharidosis type I (Hurler syndrome) following hematopoietic stem cell transplantation. Orphanet J Rare Dis 2016;11:93.

14   Visigalli I, Delai S, Politi LS et al. Gene therapy augments the efficacy of hematopoietic cell transplantation and fully corrects mucopolysaccharidosis type I phenotype in the mouse model. Blood 2010;116:5130–5139.

15   Wolf DA, Banerjee S, Hackett PB et al. Gene therapy for neurologic manifestations of mucopolysaccharidoses. Expert Opin Drug Deliv 2015;12:283–296.

16   Skvorak KJ, Dorko K, Marongiu F et al. Improved amino acid, bioenergetic metabolite and neurotransmitter profiles following human amnion epithelial cell transplant in intermediate maple syrup urine disease mice. Mol Genet Metab 2013;109:132–138.

17   Skvorak KJ, Dorko K, Marongiu F et al. Placental stem cell correction of murine intermediate maple syrup urine disease. Hepatology 2013;57:1017–1023.

18   Hong S-B, Seo M-S, Park S-B et al. Therapeutic effects of human amniotic epithelial stem cells in Niemann–Pick type C1 mice. Cytotherapy 2012;14:630–638.

19   Miki T, Grubbs B. Therapeutic potential of placenta-derived stem cells for liver diseases: Current status and perspectives. J Obstet Gynaecol Res 2014;40:360–368.

20   Sakuragawa N, Enosawa S, Ishii T et al. Human amniotic epithelial cells are promising transgene carriers for allogeneic cell transplantation into liver. J Hum Genet 2000;45:171–176.

21   Marongiu F, Gramignoli R, Dorko K et al. Hepatic differentiation of amniotic epithelial cells. Hepatology 2011;53:1719–1729.

22   Strom SC, Skvorak K, Gramignoli R et al. Translation of amnion stem cells to the clinic. Stem Cells Dev 2013;22(suppl 1):96–102.

23   Miki T, Strom SC. Amnion-derived pluripotent/multipotent stem cells. Stem Cell Rev 2006;2:133–142.

24   Parolini O, Alviano F, Bagnara GP et al. Concise review: Isolation and characterization of cells from human term placenta: Outcome of the first international Workshop on Placenta Derived Stem Cells. Stem Cells 2008;26:300–311.

25   Mamede A, Carvalho M, Abrantes A et al. Amniotic membrane: From structure and functions to clinical applications. Cell Tissue Res 2012;349:447–458.

26   Dua HS, Gomes JAP, King AJ et al. The amniotic membrane in ophthalmology. Surv Ophthalmol 2004;49:51–77.

27   Yeager AM, Singer HS, Buck JR et al. A therapeutic trial of amniotic epithelial cell implantation in patients with lysosomal storage diseases. Am J Med Genet 1985;22:347–355.

28   Cerneca F, Andolina M, Simeone R et al. Treatment of patients with Niemann-Pick type is using repeated amniotic epithelial cells implantation: Correction of aggregation and coagulation abnormalities. Clin Pediatr (Phila) 1997;36:141–146.

29   Akle CA, Adinolfi M, Welsh KI et al. Immunogenicity of human amniotic epithelial cells after transplantation into volunteers. Lancet 1981;2:1003–1005.

30   Ashton LJ, Brooks DA, McCourt PA et al. Immunoquantification and enzyme kinetics of alpha-L-iduronidase in cultured fibroblasts from normal controls and mucopolysaccharidosis type I patients. Am J Hum Genet 1992;50:787–794.

31   Garcia-Rivera MF, Colvin-Wanshura LE, Nelson MS et al. Characterization of an immunodeficient mouse model of mucopolysaccharidosis type I suitable for preclinical testing of human stem cell and gene therapy. Brain Res Bull 2007;74:429–438.

32   Miki T, Marongiu F, Dorko K et al. Isolation of amniotic epithelial stem cells. In: Current Protocols in Stem Cell Biology. T Schlaeger Ed, Chapter 1. Hoboken, NJ: Wiley, 2010:Unit 1E.3.

33   Miki T, Lehmann T, Cai H et al. Stem cell characteristics of amniotic epithelial cells. Stem Cells 2005;23:1549–1559.

34   Graupman P, Pan D, Konair B et al. Craniofacial abnormalities in a murine knock-out model of mucopolysaccharidosis I H: A computed tomography and anatomic study. J Craniofac Surg 2004;15:392–398.

35   Whitley CB, Ridnour MD, Draper KA et al. Diagnostic test for mucopolysaccharidosis. I. Direct method for quantifying excessive urinary glycosaminoglycan excretion. Clin Chem 1989;35:374–379.

36   Dunn SR, Qi Z, Bottinger EP et al. Utility of endogenous creatinine clearance as a measure of renal function in mice. Kidney Int 2004;65:1959–1967.

37   Cheetham SA, Smith AL, Armstrong SD et al. Limited variation in the major urinary proteins of laboratory mice. Physiol Behav 2009;96:253–261.

38   Lin H-Y, Shih S-C, Chuang C-K et al. Assessment of bone mineral density by dual energy X-ray absorptiometry in patients with mucopolysaccharidoses. Orphanet J Rare Dis 2013;8:71. https://ojrd.biomedcentral.com/articles/10.1186/1750-1172-8-71.

39   Rowan DJ, Tomatsu S, Grubb JH et al. Assessment of bone dysplasia by micro-CT and glycosaminoglycan levels in mouse models for mucopolysaccharidosis type I, IIIA, IVA, and VII. J Inherit Metab Dis 2013;36:235–246.

40   Pastores GM, Maegawa GHB. Clinical neurogenetics: Neuropathic lysosomal storage disorders. Neurol Clin 2013;31:1051–1071.

41   Boustany R-MN. Lysosomal storage diseases–the horizon expands. Nat Rev Neurol 2013;9:583–598.

42   Futerman AH, Meer G van. The cell biology of lysosomal storage disorders. Nat Rev Mol Cell Biol 2004;5:554–565.

43   Li Z, Yasuda Y, Li W et al. Regulation of Collagenase Activities of Human Cathepsins by Glycosaminoglycans. J Biol Chem 2004;279:5470–5479.

44   Wilson S, Hashamiyan S, Clarke L et al. Glycosaminoglycan-mediated loss of cathepsin K collagenolytic activity in MPS I contributes to osteoclast and growth plate abnormalities. Am J Pathol 2009;175:2053–2062.

45   McDonald CA., Payne NL, Sun G et al. Immunosuppressive potential of human amnion epithelial cells in the treatment of experimental autoimmune encephalomyelitis. J Neuroinflammation 2015;12:112.

46   Hori J, Wang M, Kamiya K et al. Immunological characteristics of amniotic epithelium. Cornea 2006;25(suppl 1):S53–S58.

47   Ilancheran S, Michalska A, Peh G et al. Stem cells derived from human fetal membranes display multilineage differentiation potential. Biol Reprod 2007;77:577–588.

48   Scaggiante B, Comelli M, Romeo D. Secretion of lysosomal hydrolases by cultured human amnion epithelial cells. Exp Cell Res 1991;195:194–198.

49   Clarke LA, Wraith JE, Beck M et al. Long-term efficacy and safety of Laronidase in the treatment of mucopolysaccharidosis I. Pediatrics 2009;123:229–240.

50   Wraith JE, Beck M, Lane R et al. Enzyme replacement therapy in patients who have mucopolysaccharidosis I and are younger than 5 years: Results of a multinational study of recombinant human alpha-L-iduronidase (laronidase). Pediatrics 2007;120:e37–46.

51   Di Domenico C, Di Napoli D, Gonzalez Y et al. Limited transgene immune response and long-term expression of human alpha-L-iduronidase in young adult mice with mucopolysaccharidosis type I by liver-directed gene therapy. Hum Gene Ther 2006;17:1112–1121.

52   Lai RC, Arslan F, Lee MM et al. Exosome secreted by MSC reduces myocardial ischemia/reperfusion injury. Stem Cell Res 2010;4:214–222.

53   Lai RC, Chen TS, Lim SK. Mesenchymal stem cell exosome: A novel stem cell-based therapy for cardiovascular disease. Regen Med 2011;6:481–492.

54   Ibrahim AG-EG-E, Cheng K, Marbán E. Exosomes as critical agents of cardiac regeneration triggered by cell therapy. Stem Cell Reports 2014;2:606–619.

55   Crawley EJ, Tissue C, Laboratories B et al. Transplantation of human umbilical mesenchymal stem cells cures the corneal defects of mucopolysaccharidosis VII mice. Stem Cells 2013;31:2116–2126.

See www.StemCellsTM.com for supporting information available online.